Rev.Adv.Mater.Sci. 12 (2006) 23-32

DIRECT OBSERVATION OF THE FERROMAGNETIC SPIN POLARIZATION IN GOLD NANOPARTICLES: A REVIEW

Y. Yamamoto and H. Hori

School of Materials Science, Japan Advanced Institute of Science and Technology (JAIST), 1-1 Asahidai, Tatsunokuchi, Ishikawa 923-1292, Japan

Received: November 12, 2005

Abstract. We review the magnetic properties of noble metal nanoparticles protected by polymers and the first direct evidence of the intrinsic ferromagnetism of Au nanoparticles protected by polyallyl amine hydrochloride (PAAHC) by means of element-specific magnetization (ESM) measured by X-ray magnetic circular dichroism (XMCD) spectroscopy. Unlike conventional methods, XMCD can detect magnetic moments in an element-specific manner because it is sensitive to differences between the up- and down-spin densities near the Fermi level of specific element of interest.

1. INTRODUCTION

Although nanoparticles are now used in a wide range of devices, including catalytic [1], optical [2], magnetic [3], and electronic [4], solid state properties of nanoparticles are not well understood. One main reason for this is the difficulty in controlling the size and agglomeration of the metal nanoparticles during synthesis. Size is important because, at their scale of hundreds of thousands of atoms, we are interested in effects of discrete energy levels at low temperatures [5,6] and novel surface effects due a high proportion of the atoms being on the surface. The size of the metal nanoparticles is especially difficult to control when synthesizing by vapor deposition of the metal, which produces highly pure nanoparticles that are unstable in the air and readily agglomerate. Currently, the synthesis method that best allows us to control their size is chemical reduction of metal salts; the nanoparticles' diameters within a typical sample synthesized using this method tends to vary by only a few percent of the mean diameter. To stabilize the metal nanoparticles and prevent agglomeration, the synthesis is performed in the presence of certain organic compounds, which can hamper attempts to study the intrinsic properties of the metal nanoparticles.

In this paper, we review the magnetic properties of chemically synthesized well-defined noble metal nanoparticles and element-specific magnetization study of Au nanoparticles by using the X-ray magnetic circular dichroism (XMCD) spectroscopy.

Corresponding author: Y. Yamamoto, e-mail: y-yamamo@jaist.ac.jp

Table 1. The number of atoms in the *n*th-shell cluster, the ratio of the number of the surface atoms to the total number of the atoms in the cluster, and calculated diameter of the *n*th-shell cluster for Pd and Au.

Shell number	The no. of atoms in cluster	Ratio of surface atoms	Pd diameter (nm)	Au diameter (nm)
1st	13	92%	0.72	0.75
2nd	55	76%	1.16	1.21
3rd	147	63%	1.61	1.68
4th	309	52%	2.06	2.15
5th	561	45%	2.52	2.63

2. MAGNETIC PROPERTIES OF NOBLE METAL NANOPARTICLES

Noble metal nanoparticles such as a Pd, Pt, and Au have been widely synthesized because the noble metals are easier to reduce than transition metals. These chemically synthesized metal nanoparticles are generally categorized into two subgroups, high-nuclearity metal clusters stabilized by ligands, and clusters in colloids. The former, a well-known example being the Au_{55} cluster first synthesized by Schmid [7], are stoichiometric, and have a metal core made up of successive close packed shells of metal atoms (Table 1). Each sample contains identical clusters that are cuboctahedron or truncated octahedron in shape with a face-centred cubic (FCC) crystal structure, as shown in Fig. 1. These materials are well characterized by their crystallinity, chemical stability and ideal mono-dispersed features. In particular, noble metal nanoclusters have been synthesized using various stabilizer molecules, *e.g.* $Au_{55}(PPh_3)_{12}Cl_6$, $Pd_{561}phen_{36}O_{200\pm20}$, *etc.* [8]. However, it is not possible to arbitrarily control the diameter of these samples or produce large clusters because the diameter is defined by the so-called 'magic numbers' of metal atoms in a closed shell [7].

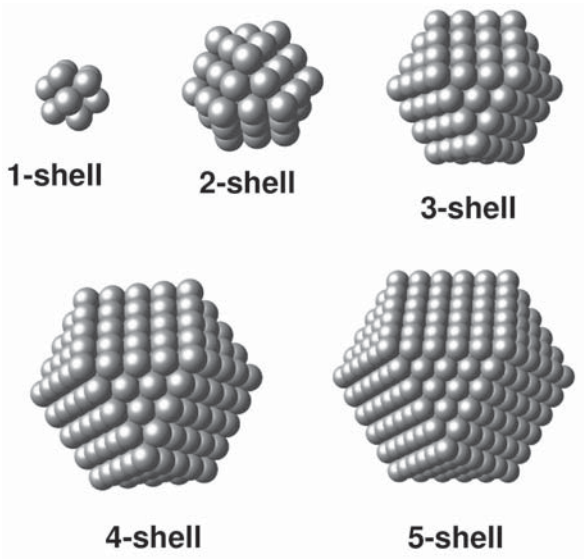

Fig. 1. Shell structure of the noble metal nanoparticles.

A colloid of metal nanoparticles is schematically shown in Fig. 2. The nanoparticles are monodispersed because they are protected by surfactants and polymers. The size of the nanoparticles can be controlled by changing the initial ratio of the amounts of metal salt and protective polymer. Using a recently developed synthesis method, the mean diameter of mono-dispersed noble metal (Pd, Pt, Au) nanoparticles embedded in linear alkyl chain polymers such as a poly(*N*-vinyl-2-pyrrolidone) (PVP) can be controlled [9,10]. Also, heat induced size control method of dodecanthiol protected Au nanoparticles was developed [11]. Fig. 3 shows high resolution TEM image of Au nanoparticles protected by dodecanthiol as a typical example. As shown in Fig. 4, Au nanoparticles maintain the fcc structure, although the Bragg peaks broaden with decreasing diameter. Thus, these method ensure the generation of mono-dispersed metal nanoparticles with arbitrary diameter. A wide range of particle diameters can be achieved and the variance in the diameter is very small. The ability of this method to adjust the size of the clusters allows a systematic investigation of the physical properties of metal clusters in the nanometer size range.

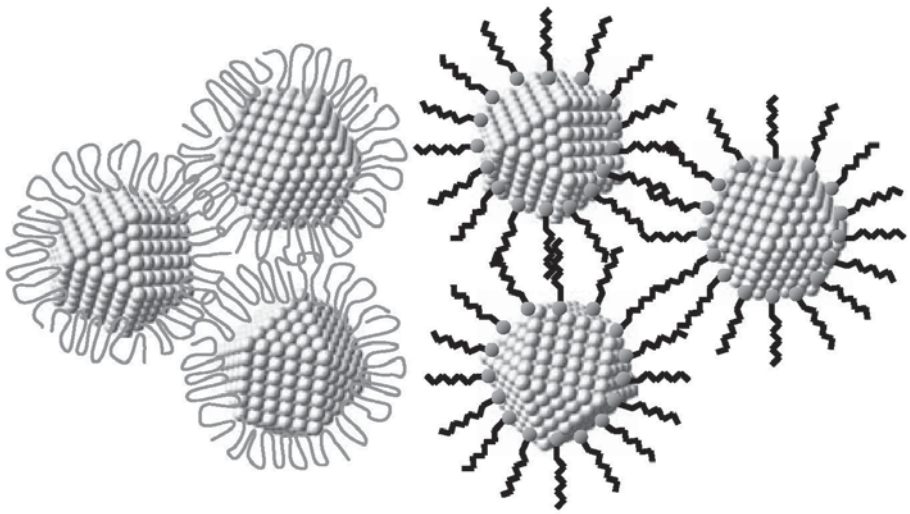

Fig. 2. Schematic illustration of the metal nanoparticles stabilized by linear polymer and surfactant.

In earlier work, we have studied giant magnetic moment effect induced by magnetic elements for the Pd/Ni core-shell (the surface atom are Ni and core atoms are Pd) nanoparticles protected by linear polymer PVP with the diameter of about 2 nm [12]. Such a nanoparticles possess ferromagnetic moments and exhibit so-called superparamagnetic behavior in the magnetization curve because the nanoparticles are so well separated that there is no magnetic interaction between them. In these nanoparticles, we found that saturation magnetization initially increases slowly with increase in the concentration of Ni, and increases very rapidly when the concentration reaches 6%. Superparamagnetic behavior was also observed for pure Pd nanoparticles with a diameter of 2.5 nm. This observation, however, was unexpected because bulk Pd metal shows Pauli paramagnetism. This means that very small Pd particles may have a ferromagnetic moment, even though Pd is normally non-magnetic. This observation cannot be explained by the so-called even-odd effect because the estimated magnetic moment is above 10 μ_B and the amount of magnetic impurity estimated by inductively coupled plasma (ICP) spectroscopy could not account for the size of magnetization. However, Pd metal is known as a 'nearly ferromagnetic metal' because of the sharp density-of-states peak near the Fermi level, and because a small magnetic impurity in the Pd metal polarizes surrounding Pd atoms, inducing a large magnetic moment. Therefore, one may ascribe this observation to an extrinsic effect due to the presence of the magnetic impurity.

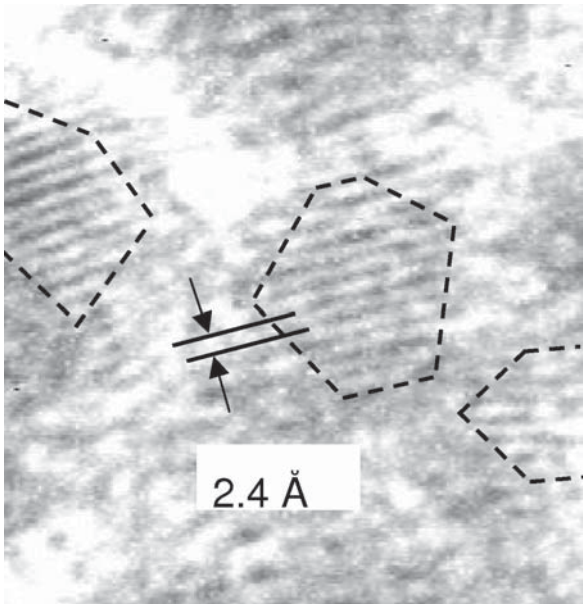

Fig. 3. High resolution TEM image of Au nanoparticles protected by dodecanthiol.

To check whether this effect occurs in other noble metal nanoparticles, we similarly investigated Pt and Au nanoparticles. In bulk, Pt shows Pauli paramagnetism and, due to a large contribution of Landau diamagnetism, Au shows diamagnetism. However, as shown in Fig. 5, superparamagnetic behaviors were observed at low temperatures for both Pt and Au nanoparticles [13,14]. Like Pd, Pt is also a 'nearly ferromagnetic metal' so there is also the possibility of magnetic moment induced by magnetic impurity. However, it is thought that such an effect is negligible in diamagnetic Au metal. Moreover, it should be noted that the observed magneti-

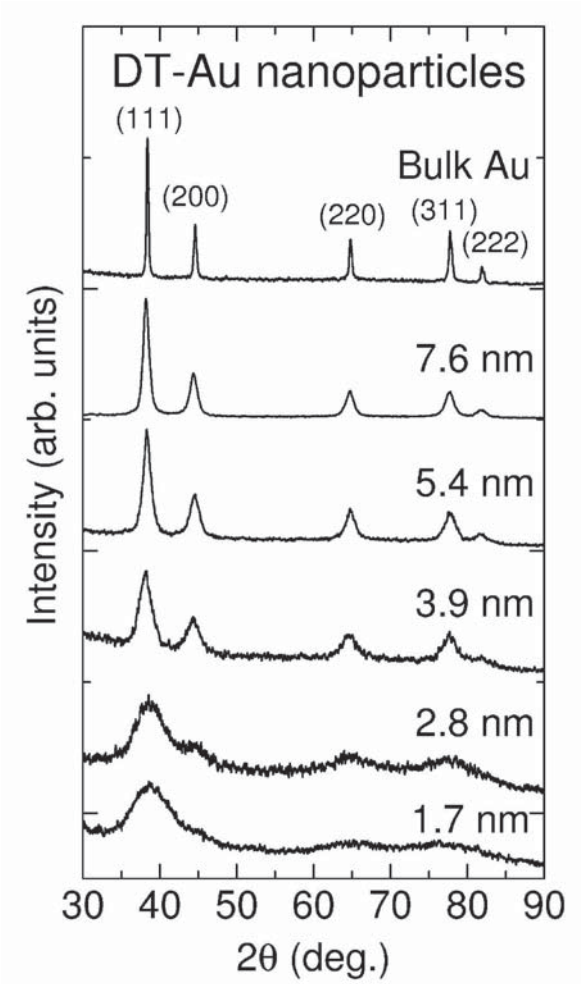

Fig. 4. X-ray diffraction patterns of DT-Au nanoparticles.

zation is dependent on the protective molecules. In a previous study, dodecanthiol-protected Au (DT-Au) nanoparticles showed much smaller magnetization than Au nanoparticles protected by polymers such as a PVP, polyacrylonitril (PAN), and polyallyl amine hydrochloride (PAAHC) [15]. Additionally, the saturation magnetization increases with decreasing diameter. These results suggest that the magnetism originates from the surface of the nanoparticles.

However, there is no clear evidence that the ferromagnetism of Au particles is intrinsic, because conventional magnetometry techniques, such as SQUID magnetization, cannot differentiate magnetization signals originating from the metal in question from those originating from magnetic impurities or unpaired electrons in the protective polymer.

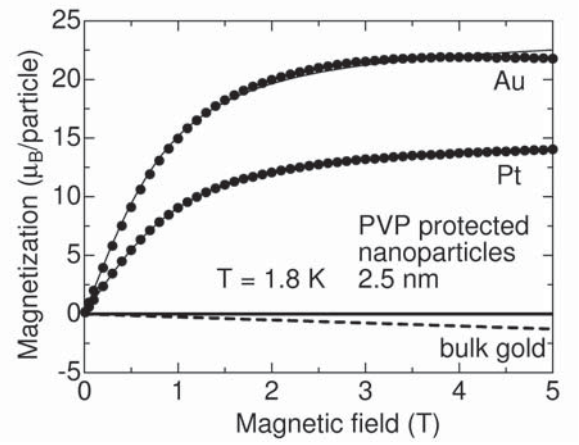

Fig. 5. Magnetization process at 1.8K for Pt and Au nanoparticles protected by PVP. Dotted line shows the magnetization process of bulk gold.

The XMCD experiments using synchrotron radiation excellently resolves above mentioned difficulties. As is well known, XMCD is a technique to measure the difference of the X-ray absorption corresponding between right circularly polarized X-ray $I(\sigma+)$ and left circularly polarized X-ray $I(\sigma-)$ by incidenting the X-ray having the energy of the absorption edge of specific element to the sample. Unlike conventional methods, XMCD is an element- and orbital-specific magnetic probe, since the signal is extracted from the X-ray absorption spectra in accordance with the 'selection rules' of the electric dipole transitions. Furthermore, by applying the magneto-optic sum rule to the spectra, the orbital moment and spin moment contributions to the total magnetic moment can be deduced separately. To date, XMCD spectroscopy has been used to investigate the magnetism of nanostructured materials [16], thin films [17] and strongly correlated systems [18] since the first observation of XMCD in Fe [19]. Therefore, we decided to use XMCD spectroscopy.

3. EXPERIMETAL

3.1. XMCD

We have recorded XMCD spectra using a highly sensitive spectrometer installed at BL39XU in SPring-8 in Japan, the world's largest third-generation synchrotron radiation facility. External magnetic fields up to 10 T were applied along the X-ray beam direction using a split-type superconducting magnet. The experimental resolution was high enough to detect XMCD signals of 10^{-5} parts of the spin-averaged X-ray absorption coefficients. This high

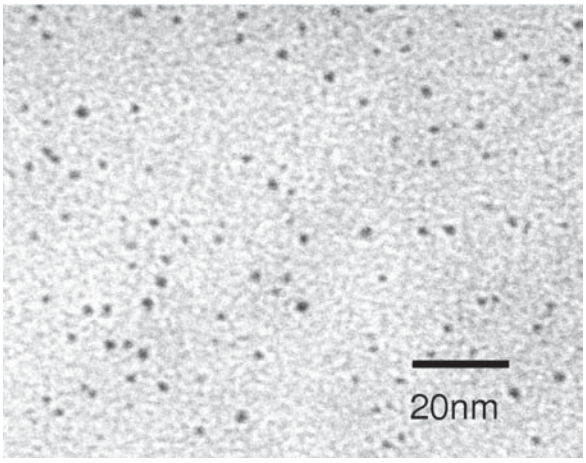

Fig. 6. TEM image of Au nanoparticles protected by PAAHC. Mean diameter of the sample is 1.9 nm. Scale bar is shown in the image.

sensitivity is achieved by excellent signal to noise ratio obtained by using the helicity-modulation technique [20], which is based on lock-in detection, and the high-brilliance of the radiation source. Helicity-modulation was crucial for the detection of extremely low ferromagnetism in the Au nanoparticles.

3.2. Sample preparation

Au nanoparticles protected by PAAHC (PAAHC-Au nanoparticles) were prepared using a method similar to that described in Ref. [9]. Briefly, an aqueous solution of $HAuCl_4$ and PAAHC were refluxed with vigorous stirring for several hours in the presence of $NaBH_4$ which reduced the Au^{3+} ions. The resultant colloidal suspension consisted of nanoparticles of Au nuclei surrounded by PAAHC which prevents aggregation and oxidation of the nanoparticles. Powdered samples were obtained by drying the colloidal suspension.

The distribution of particle diameter was determined from transmission electron microscope (TEM, Hitachi H-7100) images. The TEM samples were prepared by dropping the colloidal suspension onto a carbon-coated copper grid, and allowing the solvent to evaporate at room temperature and standard pressure. The mean diameter and standard deviation of 200 particles in the TEM images were 1.9 nm (212 atoms per cluster) and 0.2 nm, respectively (Fig. 6). The nanoparticles were confirmed by transmission X-ray powder diffraction (XRD, MAC Science) using Cu-Kα radiation to have an FCC structure.

Samples were placed in the X-ray window in a sample holder made of Cu. Conventional magnetization and susceptibility measurements were also performed using a commercial superconducting quantum interference device (SQUID) magnetometer (Quantum Design, MPMS-XL) in the temperature range of 1.8 to 300K and in a magnetic field of up to 7 T. The diamagnetic contribution arising from the PAAHC surrounding the Au was subtracted by measuring the diamagnetism of PAAHC alone.

4. RESULTS

4.1. XMCD spectra

Figs. 7a and 7b shows X-ray absorption spectroscopy (XAS) and XMCD spectra of Au at the L_3-($2p_{3/2} \rightarrow 5d_{5/2}$, $6s_{1/2}$ dipole allowed transitions) and L_2-edge ($2p_{1/2} \rightarrow 5d_{3/2}$, $6s_{1/2}$) at 2.6K in an applied magnetic field of 10 T. Owing to the helicity modulation technique, a negative XMCD signal was clearly observed at the L_3-edge (11.917 keV), whereas the XMCD signal at the L_2-edge (13.730 keV) was positive [21]. The XMCD amplitude is of the order of 10^{-4} of the XAS step height. Small negative peak structures were observed at the high-energy side of the main peaks, at 11.930 and 13.741 keV. As indicated by the dotted line in Fig. 7a, the sign of the XMCD signal reversed when the magnetic field direction was changed, verifying that the observed signal is truly of magnetic origin and does not arise from any artificial effects. To the best of our knowledge, this is the first evidence of an XMCD signal arising from Au embeded in the nonmagnetic materials consist of C, H, and N.

The XMCD peak height at the L_2-edge is less than half that at the L_3-edge. This asymmetry indicates that the Au 5*d* electrons have large orbital moment. This also suggests a large magnetic anisotropy arising from the combination of orbital moment and strong spin-orbit coupling of Au [16]. Using the sum rules [22,23], the ratio of the orbital to the spin magnetic moments was determined to be $<\mu_L>/<\mu_S> = 0.145$, which is larger than that in orbital-quenched 3*d* transition metals and is comparable to the reported values for Pd and Pt systems [24, 25]. By assuming the magnetic dipole term $<T_Z>$ was neglegiable, the ratio of orbital to spin moment, $<\mu_L>/<\mu_S>$ can be determined by using

$$\frac{<\mu_L>}{<\mu_S>} = \frac{2}{3}\frac{(A_3 + A_2)}{(A_3 - 2A_2)}, \qquad (1)$$

where the A_3, and A_2 is energy integrals of the XMCD spectra at L_3- and L_2- edge, respectively. To determine this ratio, the hole number density in the Au valence band is not required. In principle, the sum

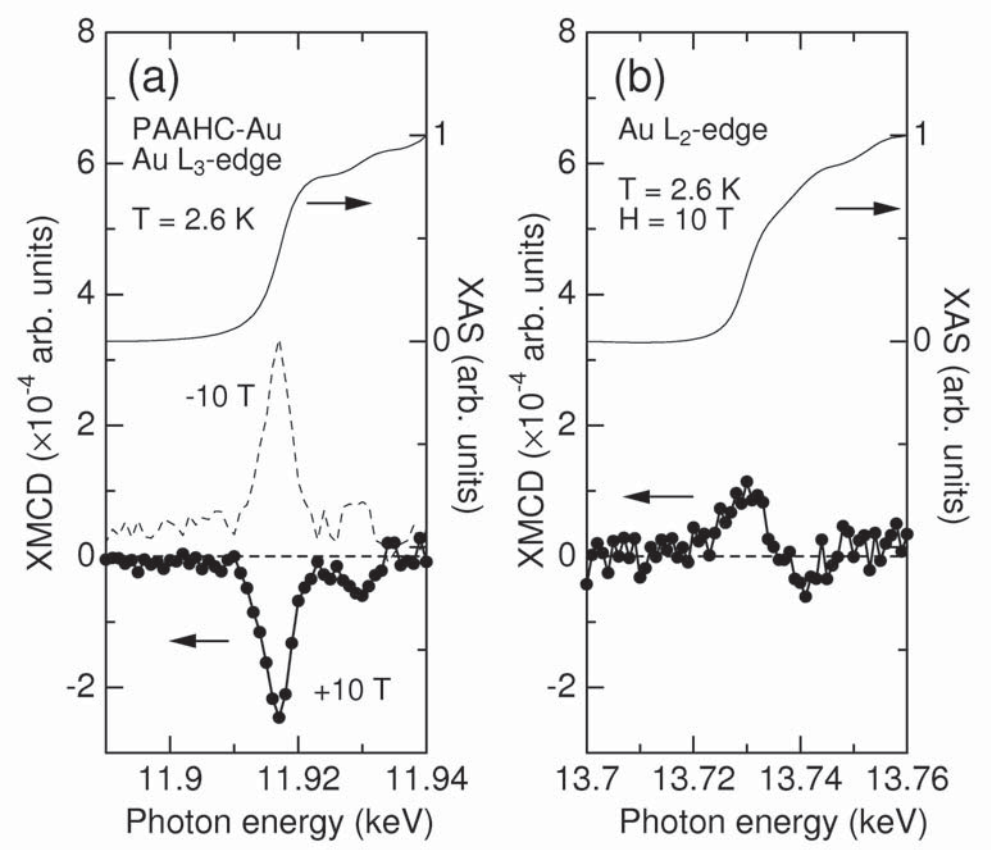

Fig. 7. XMCD and XAS spectra at (a) Au L_3- and (b) L_2-edge with an applied magnetic field of 10 T. XMCD spectra are normalized so that the height of edge jump of XAS spectra (solid lines) are unity. Dotted line represent XMCD spectra with opposite direction of applying magnetic field (-10 T).

rules give separate quantitative values of the spin and orbital magnetic moments, but require an accurate value for the hole number density and a close estimation of the $<T_Z>$ term. For Au nanoparticles, the hole number and $<T_Z>$ values are likely to be quite different from the known values for bulk Au [26], and hence we did not attempt to estimate these values. We will restrict further discussion to the element specific magnetization (ESM) obtained by the relative variations of the XMCD signal as a function of external magnetic field or temperature.

4.2. Element specific magnetization (ESM)

Taking the XMCD signal to be proportional to the magnetization, ESM is obtained by recording the peak amplitude of the XMCD spectra at the Au L_3-edge as a function of external magnetic field and temperature. Fig. 8a shows ESM measurements scaled arbitrarily for comparison with the magnetic field variation of SQUID magnetization in the same figure. ESM increases with increasing magnetic field without saturation. This behavior is similar to the magnetization process obtained by SQUID magnetization measurements.

There was no distinguishable hysteretic behavior in either the ESM or SQUID magnetization curve, while the XMCD spectra indicated a large magnetic anisotropy. We believe that this is because the superparamagnetic limit due to the small particle size obscured the magnetic anisotropy effect. As discussed in the following section, the magnetization process consists of superparamagnetic and temperature-independent Pauli-paramagnetic parts. For an ideal superparamagnetic system, the magnetization curve is expressed by $M(H)=N\mu L(x)$, with the Langevin function $L(x)=\coth(x)-1/x$, where $x=\mu H/k_B T$, μ is the magnetic moment per particle and N is the total number of particles per unit mass. Hence, the total magnetization can be expressed as $M(H)=N\mu L(x)+\chi_{Pauli}H$. The dotted line in Fig. 7a rep-

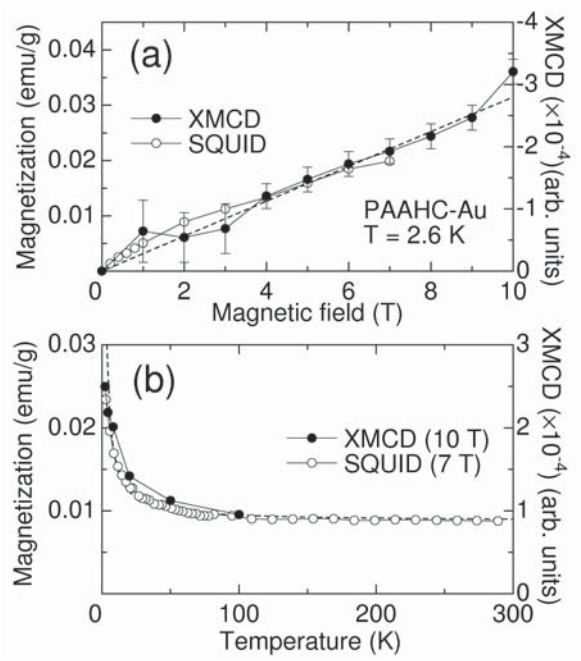

Fig. 8. (a) XMCD peak intensity of PAAHC-Au as a function of applying magnetic field and magnetization process obtained by SQUID magnetometer. The integral of the peak intensity yields similar results. Dotted line is the fit to the data assuming a Langevin function plus a linear field-dependent term. (b) Temperature dependence of XMCD peak intensity at 10 T recorded at Au L_3-edge and temperature variation of magnetization measured by SQUID magnetometer at 7 T. Dotted line is the fit to the data assuming superparamagnetism model.

resents the fitting results. The magnetic moment determined in this way was 0.4 μ_B/Au particle.

The temperature dependence of ESM was also investigated and compared with the temperature variation of the SQUID magnetization. As shown in Fig. 8b, ESM increases rapidly with decreasing temperature, although it seems that a finite constant value remains at high temperatures. The steep increase of ESM at low temperatures is consistent with the temperature variation of SQUID magnetization and does not contradict the characteristics of the superparamagnetic model (dotted line in Fig. 8b). The temperature-independent magnetization corresponds to the Pauli-paramagnetic part mentioned above. This is not observed in bulk gold metal, which shows a diamagnetic response ($-0.142 \cdot 10^{-6}$ emu/g) and monotonic increase with decreasing temperature. We believe that the paramagnetism of Au is masked in the bulk state by the huge diamagnetism of the conduction electrons, but not masked in nanoparticles because a size effect reduces the density of states at the Fermi level and consequently suppresses the diamagnetism.

The magnetization under zero field cooling (ZFC) and field cooling (FC) conditions coincide with each other, that is, blocking phenomenon was not observed. As mentioned above, superparamagnetic limit due to small size of nanoparticles is attributed to the absence of the blocking phenomenon. At the time sacle of conventional magnetization measurements, the blocking temperature T_B is given by $T_B \approx K_u V / 25k_B$, where K_u the magnetic anisotropy constant and V the volume of nanoparticles. The blocking temperature is roughly estimated to be about 1K by assuming $V = 3.6 \cdot 10^{-21}$ cm^3 and $K_u \sim 10^6$ erg/cc. This may be why we did not observe the blocking phenomenon at the lowest temperature (about 2K) in the study. We believe that the hysteresis curve can be observed by magnetization measurement at lower temperatures.

5. DISCUSSION

5.1. An origin of magnetic polarization

As XMCD is an element-selective technique, impurities do not seriously hamper the investigation of the magnetic properties of metal nanoparticles. In previous studies, XMCD has revealed induced spin polarization in nonmagnetic Cu layers in the Co/Cu multilayer system [27]. Most recently, an induced magnetic moment of 0.062 μ_B arising from Au atoms in an Au/Co multilayer system was observed by XMCD [28]. In the present study, XMCD revealed magnetization of Au in Au nanoparticles protected by PAAHC. In light of the previous studies, one might attribute the magnetization to the polarization of the Au conduction electrons induced by magnetic impurities because the absolute value of the magnetic moment is relatively small. However, this possibility can be excluded in the present system for the following reasons: i) Fe, Co or Ni were undetected by inductively coupled plasma mass spectrometry (ICP-MS) at a detectible limit of 5 ppm, and even 5 ppm Fe could not account for the magnitude of the magnetization measured by SQUID magnetometry. ii) in contrast to near ferromagnetic Pd and Pt, there has been no report of the Au conduction electrons being magnetically polarized by magnetic impurities, because in the Au nanoparticles the density of states at the Fermi level is small. iii) even if the magnetic impurities in the nanoparticles could po-

larize nonmagnetic Au atoms, the amount of magnetic impurity is far smaller (< 5 ppm) in the Au nanoparticles than in Co/Cu multilayer systems, where a Cu spacer layer adjoins a Co magnetic layer of comparable volume. Therefore, the signal in the Au nanoparticles would be too small to be detected by XMCD. Furthermore, it should be noted that our system consists of Au and a polymer matrix that is made of nonmagnetic elements (C, H, N). Therefore, we conclude that the observed magnetization is an intrinsic effect of the Au particles.

The Kubo effect cannot be responsible for the magnetization because, considering the size of the Au nanoparticles, the Kubo effect would have been observable below 1K [5]. One possible explanation for the ferromagnetic polarization is surface ferromagnetism due to the large ratio of the number of atoms on the surface to the number in the core. Although calculations including such a surface effect have been performed in few studies, it has been predicted theoretically that ferromagnetic spin polarization could take place in 4*d* and 5*d* transition metals with reduced coordination geometry [29]. Moreover, if one assumes that superparamgnetism and Pauli-paramagnetism arise from surface atoms and core atoms in Au nanoparticles respectively, the observed mixture of superparamagnetism and Pauli-paramagnetism can be reasonably explained.

5.2. Effect of protective molecules on magnetic properties

Of course, the polymers, as stabilizers of the nanoparticles, also interact with the surface and would play an important role: the electronic properties of Au particles strongly depends on the type of molecules used [30]. For example, ligand molecules with a large affinity to the metal tend to quench the magnetic moment at the surface of nanoparticles [31]. As was observed for Ni with CO chemisorption, CO strongly ligate with the surface of Ni and this affects as crystalline electric field resulting in non-magnetic spin state. In our case, PAAHC polymer has amino ($-NH_2$) functional group and the interaction between the surface of Au nanoparticles and NH_2 is considered to be weak compared to strong ligands such as mercapto (-SH) and carbonyl group (-CO). Furthermore, the Au nanoparticles in our study have far fewer ligand binding sites than do stoichiometric metal clusters such as $Au_{55}(PPh_3)_{12}Cl_6$.

As mentioned in Section 2, our recent experiments showed a sizeable reduction in the magnetization of ligand-stabilized nanoparticles such as DT-protected Au nanoparticles. By contrast, several kinds of polymer-stabilized nanoparticles exhibited similar superparamagnetic behavior with large magnetic moments [15]. This suggests that the interaction between the surface of the Au nanoparticles and the ligand is weak for polymer-stabilized nanoparticles compared with DT-protected nanoparticles, in which the ligand forms covalent bonds with the metal surface [30].

Thus, the present experimental results suggest that PAAHC-Au can be regarded as a nearly free-standing cluster, and thus the surface magnetic moment survives. This is supported by recent experimental observations of ferromagnetism or paramagnetism in large bare Pd and Au clusters produced by a vapor deposition method [32-34] and polymer protected Pd nanoparticles [35]. In contrast to our results however, it was recently reported that a SAM film with a thiol functional group induced magnetism when deposited on a Au thin film [36] and a hysteretic magnetization curve was observed for Au nanoparticles protected by molecules with a thiol functional group [37]. Nevertheless, these observations could be attributed to the charge transfer process from the surface to the molecule [26,38].

Our preliminary ESM measurement for the samples protected by DT and PAAHC showed that the amplitude of the XMCD signal for DT-Au nanoparticles was smaller than that for PAAHC-Au nanoparticles, consistent with our magnetization measurements. Therefore, we emphasize that observed spin polarization is due to the increased ratio of the surface to total atoms and the weakness of the interaction between the surface and the protective molecules.

6. CONCLUSION

In conclusion, our XMCD and ESM experiments have revealed intrinsic magnetic polarization in Au nanoparticles with a mean diameter of 1.9 nm. The external magnetic field and temperature dependence of the ESM signal suggested that magnetization of Au nanoparticles consists of a superparamagnetic part obeying the Curie law, and a temperature-independent Pauli-paramagnetic part. The mixture of these components can be reasonably explained by considering the surface atoms to be ferromagnetic and the core atoms to be Pauli-paramagnetic. We infer that the weak coupling between the protective agent and the gold surface is a prerequisite for the observation of spin polarization.

Due to the high ratio of the surface atoms to the constituent atoms and the capability of the chang-

ing the capping organic molecules, metal nanoparticles protected by organic molecules will provide an variety of research fields such as magnetism related to the electron transfer between organic molecules and metal surface, and the physics and chemistry of surface and interfaces. The XMCD technique will be a powerful tool for this kind of study.

ACKNOWLEDGEMENTS

This work was supported by the Inoue foundation of Science and the Special Coordination Funds for Promoting Science and Technology by the Ministry of Education, Culture, Sports, Science, and Technology (MEXT). The synchrotron radiation experiments were performed at SPring-8 with the approval of Japan Synchrotron Radiation Research Institute (JASRI) as Nanotechnology Support Project of The Ministry of Education, Culture, Sports, Science and Technology (Proposal No. 2002B0380-NS2-np / BL-No.39XU).

REFERENCES

[1] M. Valden, X. Lai and T. Goodman // *Science* **281** (1998) 1647.

[2] H.-G. Boyen, G. Kästle, F. Weigl, B. Koslowski, C. Dietrich, P. Ziemann, J. P. Spatz, S. Riethmüller, C. Hartmann, M. Möller, G. Schmid, M. G. Garnier and P. Oelhafen // *Science* **297** (2002) 1533.

[3] S. Sun, C. B. Murray, D. Weller, L. Folks and A. Moser // *Science* **287** (2000) 1989.

[4] R. P. Andres, J. D. Bielefeld, J. I. Henderson, D. B. Janes, V. R. Kolagunta, C. P. Kubiak, W. J. Mahoney and R. G. Osifchin // *Science* **273** (1996) 1690.

[5] Y. Volokitin, J. Sinzig, L. J. de Jongh, G. Schmid, M. N. Vargaftik and I. I. Moiseevi // *Nature* **384** (1996) 621.

[6] *Physics and Chemistry of Metal Cluster Compounds*, ed. by L. J. de Jongh (Kluwer, Dordrecht, 1994).

[7] *Cluster and Colloids. From Theory to Applications*, ed. by G. Schmid (VCH, Weinheim, 1994).

[8] G. Schmid // *Polyhedron* **7** (1988) 2321.

[9] T. Teranishi, I. Kiyokawa and M. Miyake // *Adv. Mater.* **10** (1998) 596.

[10] T. Teranishi and M. Miyake // *Chem. Mater*. **11** (1999) 3414.

[11] T. Teranishi, S. Hasegawa, T. Shimizu and M. Miyake // *Adv. Mater.* **13** (2001) 1699.

[12] N. Nunomura, H. Hori, T. Teranishi, M. Miyake and S. Yamada // *Phys. Lett.* **A249** (1998) 524.

[13] H. Hori, T. Teranishi, Y. Nakae, Y. Seino, Y. Miyake and S. Yamada // *Phys. Lett.* **A263** (1999) 406.

[14] Y. Yamamoto, T. Miura, Y. Nakae, T. Teranishi, M. Miyake and H. Hori // *Physica B* **329-333** (2003) 1183.

[15] H. Hori, Y. Yamamoto, T. Iwamoto, T. Miura, T. Teranishi and M. Miyake // *Phys. Rev. B* **69** (2004) 174411.

[16] P. Gambardella, A. Dallmeyer, K. Maiti, M. C. Malagoli, W. Eberhardt and K. Kern // *Nature* **416** (2002) 301.

[17] D. Weller, J. Stöhr, R. Nakajima, A. Carl, M. G. Samant, C. Chappert, R. Mégy, P. Beauvillain, P. Veillet and G. A. Held // *Phys. Rev. Lett.* **75** (1995) 3752.

[18] M. Kučera, J. Kuneš, A. Kolomiets, M. Diviš, A. V. Andreev, V. Sechovský, J.-P. Kappler and A. Rogalev // *Phys. Rev. B* **66** (2002) 144405.

[19] G. Schütz, W. Wagner, W. Wilhelm, P. Kienle, R. Zeller, R. Frahm and G. Materik // *Phys. Rev. Lett.* **58** (1987) 737.

[20] M. Suzuki, N. Kawamura, M. Mizumaki, A. Urata, H. Maruyama, S. Goto and T. Ishikawa // *Jpn. J. Appl. Phys.* **36** (1998) L1488.

[21] Y. Yamamoto, T. Miura, M. Suzuki, N. Kawamura, H. Miyagawa, T. Nakamura, K. Kobayashi, T. Teranishi and H. Hori // *Phys. Rev. Lett.* **93** (2004) 116801.

[22] B. T. Thole, P. Carra, F. Sette and G. van der Laan // *Phys. Rev. Lett.* **68** (1992) 1943.

[23] P. Carra, B. T. Thole, M. Altarelli and X. Wang // *Phys. Rev. Lett.* **70** (1993) 694.

[24] J. Vogel, A. Fontaine, V. Cros, F. Petroff, J. Kappler, G. Krill, A. Rogalev and J. Goulon // *Phys. Rev. B* **55** (1997) 3663.

[25] F. Wilhelm, P. Poulopoulos, G. Ceballos, H. Wende, K. Baberschke, P. Srivastava, D. Benea, H. Ebert, M. Angelakeris, N. K. Flevaris, D. Niarchos, A. Rogalev and N. B. Brookes // *Phys. Rev. Lett.* **85** (2000) 413.

[26] P. Zhang and T. K. Sham // *App. Phys. Lett.* **81** (2002) 736.

[27] M. G. Samant, J. Stöhr, S. S. P. Parkin, G. A. Held, B. D. Hermsmeier, F. Herman, M. Van Schilfgaarde, L.-C. Duda, D. C. Mancini, N. Wassdahl and R. Nakajima // *Phys. Rev. Lett.* **72** (1994) 1112.

[28] F. Wilhelm, M. Angelakeris, N. Jaouen, P. Poulopoulos, E. Th. Papaioannou, Ch. Mueller, P. Fumagalli, A. Rogalev and N. K. Flevaris // *Phys. Rev. B* **69** (2004) 220404(R).
[29] S. Blügel // *Phys. Rev. B*. **51** (1995) 2025.
[30] P. Zhang and T. K. Sham // *Phys. Rev. Lett.* **90** (2003) 245502.
[31] D. A. van Leeuwen, J. M. van Ruitenbeek, L. J. de Jongh, A. Ceriotti, G. Pacchioni, O. D. Häberlen and N. Rösch // *Phys. Rev. Lett.* **73** (1994) 1432.
[32] T. Taniyama, E. Ohta and T. Sato // *Europhys. Lett.* **38** (1997) 195.
[33] T. Shinohara, T. Sato and T. Taniyama // Phys. Rev. Lett. **91** (2003) 197201.
[34] W.-H. Li, S. Y. Wu, C. C. Yang, S. K. Lai, K. C. Lee, H. L. Huang and H. D. Yang // *Phys. Rev. Lett.* **89** (2002) 135504.
[35] B. Sampedro, P. Crespo, A. Hernando, R. Litrán, J. C. Sánchez-López, C. López Cartes, A. Fernandez, J. Ramírez, J. González Calbet and M. Vallet // *Phys. Rev. Lett.* **91** (2003) 237203.
[36] I. Carmeli, G. Leitus, R. Naaman, S. Reich and Z. Vager // *J. Chem. Phys.* **118** (2003) 10372.
[37] P. Crespo, R. Litrán, T.C. Rojas, M. Multigner, J. M. de la Fuente, J. C. Sánchez-López, M. A. García, A. Hernando, S. Penadés and A. Fernández // *Phys. Rev. Lett.* **93** (2004) 087204.
[38] H. Häkkinen, R. N. Barnett and U. Landman // *Phys. Rev. Lett*. **82** (1999) 3264.